Field observations of alongshore runup variability under dissipative conditions in presence of a shoreline sandwave

Nadia Senechal, Giovanni Coco, Nathaniel Plant, Karin R. Bryan, Jenna Brown, Jamie H. M. Macmahan

Journal of Geophysical Research: Oceans

RESEARCH ARTICLE
10.1029/2018JC014109

Key Points:
- Alongshore variations in runup (by a factor up to 3) are observed in presence of a shoreline sandwave mirrored in the inner sandbar
- Alongshore variations in runup are essentially driven by rapid and significant modification in the incident wave pattern rather than by foreshore beach slope $\beta_{2\sigma}$ variation
- Observed alongshore coherence length scales are consistent with the typical length scale of the morphology

Supporting Information:
- Supporting Information S1

Correspondence to:
N. Senechal,
nadia.senechal@u-bordeaux.fr

Citation:
Senechal, N., Coco, G., Plant, N., Bryan, K. R., Brown, J., & MacMahan, J. H. M. (2018). Field observations of alongshore runup variability under dissipative conditions in the presence of a shoreline sandwave. *Journal of Geophysical Research: Oceans*, *123*, 6800–6817. https://doi.org/10.1029/2018JC014109

Received 24 APR 2018
Accepted 18 AUG 2018
Accepted article online 28 AUG 2018
Published online 22 SEP 2018

Field Observations of Alongshore Runup Variability Under Dissipative Conditions in the Presence of a Shoreline Sandwave

Nadia Senechal[1], Giovanni Coco[2], Nathaniel Plant[3], Karin R. Bryan[4], Jenna Brown[3], and Jamie H. M. MacMahan[5]

[1]University Bordeaux, OASU, UMR CNRS EPOC, Talence, France, [2]The University of Auckland, Auckland, New Zealand, [3]St. Petersburg Coastal and Marine Science Center, U.S. Geological Survey, St. Petersburg, FL, USA, [4]School of Science, University of Waikato, Hamilton, New Zealand, [5]Nearshore Processes Laboratory, Naval Postgraduate School, Monterey, CA, USA

Abstract Video measurements of runup were collected at low tide along several profiles covering an alongshore distance of 500 m. The morphology displayed a complex shape with a shoreline sandwave in the lower beach face of about 250 m long mirrored in the inner sandbar. Wave conditions were stationary and moderate (offshore height of 2 m and peak period of nearly 13 s) but yet dissipative. Runup energy was dominated by infragravity frequencies. Alongshore variations in runup (by a factor up to 3) observed both in the incident and infragravity bands were much higher than reported previously (e.g., Guedes et al., 2012, https://doi.org/10.1016/j.csr.2012.08.022; Ruggiero et al., 2004, https://doi.org/10.1029/2003JC002160) while the alongshore variations in other environmental parameters (e.g., foreshore beach slope) appear to be much lower. Our data suggest that the beach morphology in the inner surf zone plays a crucial role by inducing rapid and significant modification in the incident wave pattern and the alongshore coherence length scales were consistent with the typical alongshore length scale of the morphology.

Plain Language Summary The topic of this work is to present new field data focusing an alongshore variation of the runup. The runup is the time-varying position of the water's edge on the foreshore of the beach. This parameter is crucial in better forecasting coastal hazards (e.g., coastal flooding and erosion) and coastal structure defense design.

1. Introduction

Wave-induced runup is defined as the time-varying position of the water's edge on the foreshore of the beach, resulting from a (quasi) steady component above the still water level (the wave setup) and a time-varying fluctuating component (the *swash*). Wave-induced runup is an important process driving nearshore hydrodynamics and sediment transport. In particular, runup is required to estimate extreme water levels and associated effects of coastal flooding hazards by overwash (e.g., Blenkinsopp et al., 2016; Cohn & Ruggiero, 2016; Hughes et al., 2010; Peregrine & Williams, 2001; Rodrigues et al., 2012; Serafin & Ruggiero, 2014). In addition, runup also plays a critical role in coastal changes, as the transition area between the surf zone and the subaerial beach, the swash zone, is an important part of the littoral sediment budget (e.g., Elfrink & Baldock, 2002; Houser, 2009). Under energetic conditions, runup can lead to dramatic beach and dune erosion (e.g., Palmsten & Splinter, 2016; Ruggiero et al., 2001; Sallenger, 2000; Suanez et al., 2015, 2016). Runup has thus received increasing interest over the past decade, with a focus on runup predictions based both on observations and numerical and parametric models (e.g., Atkinson et al., 2017; Cox et al., 2013; Nicolae Lerma et al., 2016, 2017; Ruju et al., 2014; Senechal, Coco, et al., 2011; Stockdon et al., 2006, 2014) with applications for coastal vulnerability assessments (e.g., Cohn & Ruggiero, 2016; Medellin et al., 2016; Stockdon et al., 2007; Vousdoukas et al., 2012) and coastal structure defense design (e.g., Arns et al., 2017; Briganti et al., 2005; Hawkes et al., 2002). Predicting wave runup still remains extremely challenging, such that there continue to be discrepancies between even the most recently developed formulations (e.g., Stockdon et al., 2006, 2014) and observed variability; these formulas still neglect a number of processes especially due to the lack of data to evaluate the benefit of new parameterizations (Plant & Stockdon, 2015).

Earlier studies have highlighted that swash characteristics (often summarized in terms of *vertical runup height*, *R*) were primarily related to offshore wave characteristic and beach slope (e.g., Guza et al., 1984; Guza & Thornton, 1982; Holman, 1986; Holman & Sallenger, 1985; Meyer & Taylor, 1972; Miche, 1951). Thus, similarly to the surf zone approach, the Iribarren number (Battjes, 1974), defined as

$$\xi_0 = \frac{\tan\beta}{(H_0/L_0)^{1/2}} \tag{1}$$

where β is the beach slope, L_0 is the deep water wavelength given by linear theory, and H_0 is the offshore significant wave height, has been commonly used to classify the swash into either dissipative, intermediate, or reflective. Dissipative conditions are commonly characterized by low Iribarren numbers, typically less than 0.3 (e.g., Guza & Thornton, 1982; Raubenheimer et al., 1995; Raubenheimer & Guza, 1996; Ruessink et al., 1998; Ruggiero et al., 2001; Stockdon et al., 2006), whereas intermediate and reflective conditions are characterized by larger values (Guedes et al., 2012; Holland, 1995; Holland & Holman, 1999; Holman, 1986; Holman & Sallenger, 1985).

Senechal, Coco, et al. (2011) pointed out that the Iribarren number, initially developed for laboratory plane beaches, can be misleading as its application to field studies requires a single beach slope value to characterize the whole cross-shore profile. In most previous works (e.g., Gomes da Silva et al., 2018; Guedes et al., 2011, 2012; Ruggiero et al., 2001; Senechal, Coco, et al., 2011; Stockdon et al., 2006), the beach slope β was defined as the $\beta_{2\sigma}$, which is the linear slope within the region between ± two standard deviations from the mean runup elevation. However, Senechal, Coco, et al. (2011) pointed out that in their study, the steep slopes characterizing the swash zone were in contrast with the mildly sloping surf zone; as a result, the swash zone experienced nearly reflective conditions while the surf zone was in a dissipative state. Recently, Hughes et al. (2014) explored the morphodynamic controls on the nature of the swash spectrum by synthesizing a large data set gathered from a broad range of microtidal beaches (reflective, intermediate, and dissipative) under low to energetic wave conditions. Their analyses demonstrated that many characteristics of swash behavior were directly or indirectly (through a relation with beach gradient) related to the beach state; however, they also underlined that the occasional lack of clear connection might be linked to a misleading classification of the beach state. Stockdon et al. (2006) also defined a surf zone beach slope β_{sz} calculated for each timestack as the slope between the shoreline and the cross-shore location of wave breaking. However, in the presence of pronounced nearshore troughs and interrupted breaking processes between the inner bar and the shoreface, this definition may be complicated to use. So while the role of offshore characteristics is well defined, the relation between beach slope and swash (in terms of vertical component of runup, *R*) remains elusive (e.g., Guedes et al., 2011). At a larger scale, Cohn and Ruggiero (2016) used a numerical approach (XBeach) to show that there is a morphologic control on swash processes on dissipative beaches, essentially from intertidal and supratidal morphology. In their experiments simulating storm conditions, natural interannual variability in beach topography explained about 80% of the variance in runup. In particular, the presence of nearshore bars may substantially affect the runup response, consistent with previous results obtained by Cox et al. (2013).

Swash spectra are generally separated into two bands that are forced by different processes: an infragravity band (typically associated with $f < 0.05$ Hz) and an incident band (typically associated with $f > 0.05$ Hz). While the incident band of runup (R_{in}) generally shows a significant relation with β under both reflective and dissipative conditions (Ruggiero et al., 2004; Senechal, Coco, et al., 2011; Stockdon et al., 2006), the relation between the infragravity band of runup (R_{ig}) and the beach slope is a matter of debate with published results from different field sites indicating contrasting behaviors. Under reflective to intermediate conditions, Stockdon et al. (2006) found no significant relationship between R_{ig} and β, while Guedes et al. (2011) found some. Under dissipative conditions, when the swash spectra are generally dominated by the infragravity band (e.g., Holman & Bowen, 1984; Ruessink et al., 1998; Ruggiero et al., 2004; Stockdon et al., 2006; Senechal, Coco, et al., 2011), Ruggiero et al. (2004) observed a strong correlation between β and R_{ig}, while Ruessink et al. (1998) and Senechal, Coco, et al. (2011) found that R_{ig} scaled better with a parameter that did not include β. Passarella et al. (2018), applying the machine learning technique from genetic programming on a large data set including a wide range of conditions from reflective to dissipative, found that the beach slope is a relevant parameter when predicting the infragravity component. In contrast, Gomes da

Silva et al. (2018) suggested using the horizontal cross-shore component of the infragravity swash instead of the associated vertical component and found it to be related to the foreshore slope (defined as $\beta_{2\sigma}$) and the morphodynamic beach state through the nondimensional fall velocity parameter.

Infragravity motions are generated by nonlinear interactions between high-frequency wind waves (Herbers et al., 1995; Longuet-Higgins & Stewart, 1962; Ruessink, 1998) whose strength is modulated by the level of offshore wave energy, the shape of the associated energy spectrum (e.g., De Bakker et al., 2015; Norheim et al., 1998), and the directional spread (e.g., Herbers & Burton, 1997). Dissipation and reflection are also processes not entirely understood (e.g., De Bakker et al., 2014). Okhiro and Guza (1995) highlighted how tidal variations of the surf zone width and beach slope might affect infragravity generation, dissipation, or reflection. Thomson et al. (2006), analyzing field observations, showed that the bottom profile affects infragravity wave energy loss close to the shoreline. Specifically, they showed infragravity energy being transferred to higher-frequency motions in the surf zone through near-resonant nonlinear interactions between triads of wave components (i.e., a reversal of the infragravity generation mechanism) was enhanced over a convex low-tide bottom profile (compared with a concave high-tide profile). De Bakker et al. (2015) used a numerical approach and laboratory data to show that the beach slope affects the nonlinear infragravity-wave interactions. Van Gent and Giarrusso (2005) showed using a numerical model that the percentage of infragravity energy generated during wave breaking also depends on the ratio of offshore wave height to the mean water depth within one wavelength of the coast.

Surprisingly, only a limited number of studies have focused on alongshore variability in runup. Holland and Holman (1999) explored the wavenumber-frequency structure of infragravity swash motions using 26 cross-shore transects spaced every 10 m in the longshore, thus covering a total alongshore distance of 260 m. However, they did not provide estimates of alongshore variability in runup parameters. In 2004, Ruggiero et al. explored alongshore variations in runup parameters over a large alongshore distance (1,600 m). In their study, they experienced dissipative conditions in the presence of a relatively alongshore uniform morphology characterized by sandbars located up to several hundred meters from the shoreline. They found the runup to be dominated by the infragravity band and linearly dependent on the local foreshore beach slope. Guedes et al. (2012) reported observations of alongshore variability of swash motions on a barred beach in the presence of moderate swell. In their study, runup was dominated by the incident component. While the incident band of the runup was well correlated to both the foreshore beach slope and the wave dissipation patterns, the infragravity component of the runup was not. Finally, Ciriano et al. (2005) and Bryan and Coco (2010) provided evidence of the nonlinear coupling between cuspate morphology and swash motions. Ciriano et al. (2005) showed evidence that beach cusp evolution might control low-mode edge wave dynamics, while Bryan and Coco (2010) concluded that the presence of cusps may enhance interactions between successive runup events at cusp horns and lead to the growth of an infragravity wave whose wavelength would be forced by the presence of the beach cusps.

The limited studies on alongshore variability represent two extremes of small spatial scales (beach cusps) and very long variations over whole beach scales. In this study, new field data of alongshore variability associated with medium-scale features that characterize strong three-dimensional (3D) bar morphology (such as transverse bar and rip, and crescentic bar cases, where pronounced shoreline embayments are commonplace) are presented for moderate energy, yet dissipative conditions. The data presented here were collected at low tide and cover an alongshore distance of 500 m in the presence of a shoreline sandwave in the lower beach face of about 250 m long mirrored in the inner sandbar. In contrast, the upper beach face was relatively uniform. The methods section describes runup data acquisition and describes the spatial, temporal, and spectral analysis methods. Then the results present evidence of significant alongshore variability in the runup. The discussion aims to investigate the question of whether the alongshore beach face slope variations or alongshore variations in surf zone morphology (which drive focusing and changes to energy transfers) are a greater driver of alongshore runup variation. Our primary findings are reviewed in the conclusions.

2. Methods

Data presented in this work were obtained during the ECORS-Truc Vert'08 Beach experiment (France). The field experiment lasted 6 weeks, from 3 March to 13 April 2008. Truc Vert'08 was designed to measure

beach modifications with emphasis on large winter waves, 3D morphology, and macrotidal conditions. Hydrodynamic processes, sediment characteristics and transport, and morphodynamics of the beach were measured over many spatial and temporal scales and are summarized in Senechal, Abadie, et al. (2011).

2.1. Field Area

The field site (Figure 1) is situated on the southern part of the French Atlantic coastline and is typical of the relatively natural coast extending 100 km between the Gironde Estuary (90 km to the north) and the Arcachon inlet (10 km to the south). This sandy coast is bordered by high aeolian foredunes (Figure 1). The sediment consists primarily of medium-grained quartz sand whose mean surface grain size varies with the morphology, with coarser sediments (~0.6 mm) observed in the deeper rip channels and finer sediments (~0.3 mm) observed on the shoals between the rips (Gallagher et al., 2011). Truc Vert beach exhibits complex 3D and highly dynamic morphology commonly involving two distinct sandbar systems. The inner bar (see Figure 1) can experience all the states within the intermediate classification (see Masselink & Short, 1993; Wright et al., 1984) and usually exhibits a Transverse Bar and Rip morphology (Senechal et al., 2009). The outer bar system exhibits long-term persistent crescentic patterns at a narrow range of wavelengths, and the shape of which varies from symmetric to asymmetric (Castelle et al., 2007). The shoreline can also exhibit significant deviations from linear behavior including, for example, the presence of sandwaves (see Figure 1). The field site experiences an annual mean spring tidal range of 3.7 m. Alongshore tide-driven currents in the nearshore zone are essentially negligible. The wave climate is energetic with an annual mean significant wave height of 1.36 m and mean period around 8 s associated with long distance swells traveling mainly from N-NW directions. The wave climate has a clear seasonal dependence with higher waves in winter than in summer (see Butel et al., 2002, for a complete wave classification of the Aquitanian coast). During the experiment, waves ranged from small swells (offshore significant heights, H_0, ranging from 0.3 to 2 m and peak periods, T_p, between 12 and 16 s) to heavy swells with a maximum H_0 of 8.1 m, on 10 March, associated with a peak period ranging from 16 to 18 s.

2.2. Measurements

Sea state conditions were measured with a directional Mark III Datawell waverider buoy anchored in 20-m depth situated offshore of the field area, about 1.5 km from the beach face. Eulerian instrumentation was deployed in the intertidal surf zone to describe the mean and surf zone scale fluctuating motions at temporal scales of $>$20 s. A synchronous, 15-Hz coherent seven-element alongshore-lagged array of colocated pressure and horizontal digital electromagnetic velocity sensors (hereafter PUV) mounted to pipes jetted along the inner bar was deployed to record the alongshore wave numbers and frequencies for intertidal surf zone infragravity motions and very low frequency motions. The instruments were located approximately 35 cm from the seabed. All instruments were cabled to the shore and time-synced to an onshore GPS clock.

Throughout the experiment, swash motion was measured with a video system mounted on an 8-m-high scaffold built on the top of the dune backing the beach and time-synced to a GPS clock. The height of the camera above mean sea level was about 27 m. The system contained two high-resolution digital cameras. Overlap in the field of view of the two cameras allowed for continuous coverage of the swash-zone so that, overall, an alongshore distance of approximately 600 m at high spring tide could be covered. The sampling frequency of the video system and of the derived runup time series was 2 Hz. The transects where the swash motions were measured were located at the same alongshore location as the PUV sensors deployed along the inner bar system (Figure 1). The runup along the selected transects was manually digitized by two operators. The same methodology as presented in Senechal, Coco, et al. (2011) was applied. Runup and rundown were identified as a white edge moving back and forth in the swash zone. To extract runup elevations along individual transects accurately from video, the topography of the beach is needed in addition to the geometry of the cameras. To obtain the beach surface topography, a survey using Real Time Kinematic Differential Global Positioning System was performed at each low tide (see Parisot et al., 2009, for a full description). Photogrammetric relationships (Holland et al., 1997) were used to convert the digitized swash into elevation time series relative to the French National datum. The vertical resolution of the runup elevation, depending both on lens properties and distance from the cameras, was estimated by mapping the horizontal pixel resolution (typically $<$1.0 m) to the elevation along the cross-shore transect. The vertical resolution was less than 0.10 m for all the data analyzed in this work.

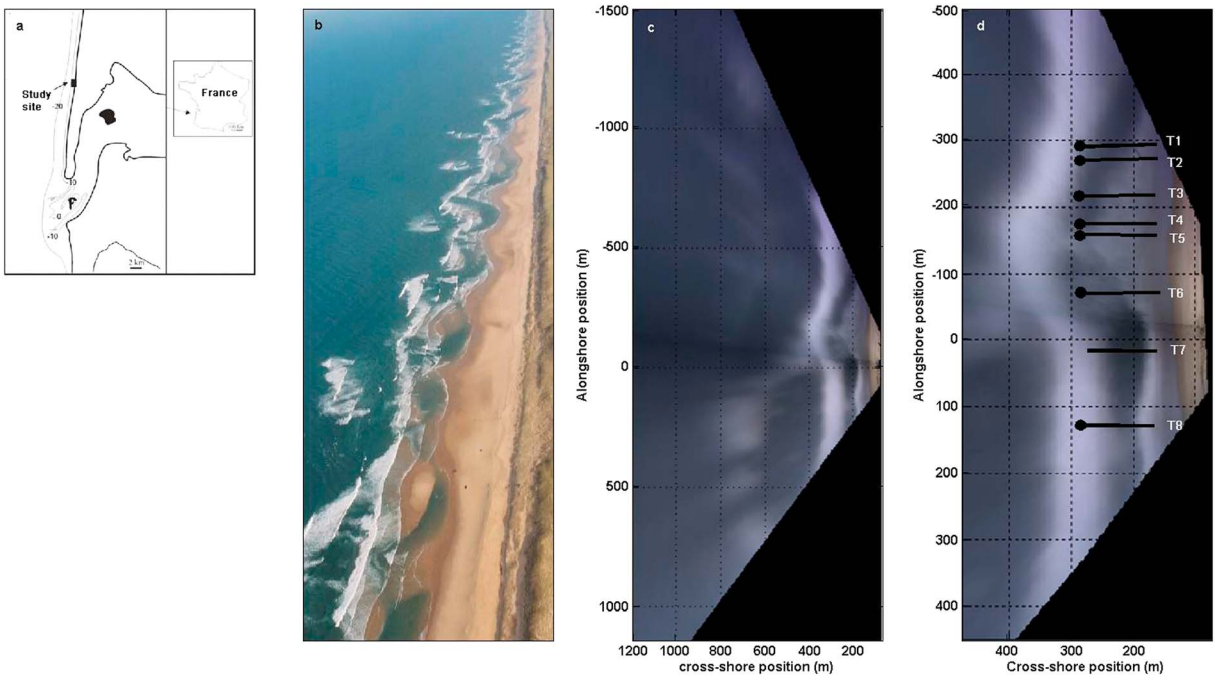

Figure 1. (a) Location of the study site. (b) Oblique aerial view of the Aquitanian coast at low tide. (c) Rectified and merged time-averaged image of the field area at low tide on 14 March. (d) Enlarged view of the inner bar. The solid lines represent the transect positions where the runup time series have been estimated from video. The black marks represent the positions of the synchronized PUV sensors. We observe a shoreline sandwave in the lower beach face (situated between transects T1 and T6) of about 250 m long mirrored in the inner sandbar.

2.3. Data Analysis

Energy spectra, PSD (f), were computed from detrended, tapered data segments of 1,800 points (900 s). The runup and surf zone data were then partitioned to determine the incident band component (0.05 Hz $< f <$ 0.24 Hz) and the infragravity band component (0.004 Hz $< f <$ 0.05 Hz). Runup, R, and surf zone wave heights, H, were calculated as follows:

$$R,\ \ H = 4^{*}\sqrt{\sum_{f_1}^{f_2}\mathrm{PSD}(f)\mathrm{d}f} \tag{2}$$

Runup and surf zone heights in the incident band (respectively R_{inc} and H_{inc}) and in the infragravity band (respectively R_{ig} and H_{ig}) were calculated by summing only over frequencies within the specified limits.

The distance between the shoreline and the inner bar crest was estimated by measuring the mean shoreline position and the bar crest position. To estimate both positions, we used time-exposure images (typically averaged over a 10-min window). The advantage of time-exposure images is that they remove visual features related to individual waves, and we can use the appearance of white bands related to the predominant wave breaking on the time-exposure images as a proxy of the submerged surf zone sandbar (Holland et al., 1997; Lippmann & Holman, 1989; Van Enckevort & Ruessink, 2001). The predominant wave breaking position was manually digitized tracking the cross-shore location of the image intensity peaks in the alongshore direction. Finally, the definition of the foreshore beach slope $\beta_{2\sigma}$ in this study was taken, in agreement with other studies of swash zone hydro- and morphodynamics (e.g., Coco et al., 2004; Ruggiero et al., 2004; Senechal, Coco, et al. 2011) to be the linear slope within the region between ± two standard deviations around the mean runup elevation.

The data discussed below consist of 120 15-min wave and runup elevation time series centered on low tide and measured along eight individual cross-shore transects. The mean water level elevations for the time series considered in this study, according to in situ pressure measurements, varied by less than 0.4 m.

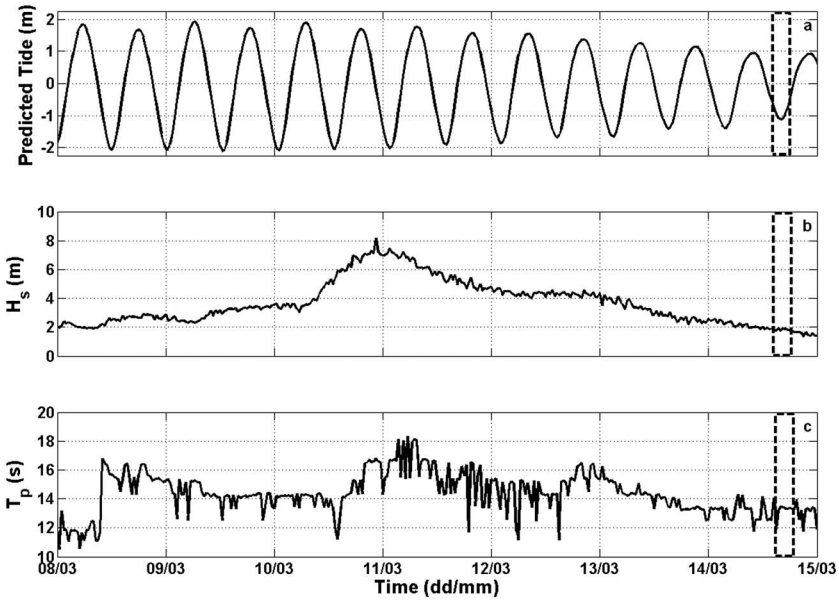

Figure 2. Environmental conditions. Data discussed here were collected during a 4-hr window (dashed box on 14 March) centered on low tide under neap tide conditions and stationary offshore wave conditions. (upper) Predicted tide. (middle) Significant offshore wave height measured by the wave buoy in about 20-m water depth. (lower) Offshore peak period.

3. Results

3.1. Environmental Conditions

An overview of offshore environmental parameters is provided in Figure 2. The period corresponds to the stationary period experienced during the low tide of 14 March (see rectangle). The stationarity experienced during this period associated with neap tide conditions provided weak variations in mean sea surface elevation (typically less than 0.4 m) over the 4-hr period, thus limiting variations in the effective swash topography and surf zone bathymetry. Conditions during this period were moderate compared to the storm experienced by the area 3 days previously. The mean offshore significant wave height was nearly 2 m, and the incident wave period was relatively long with a mean value of 13 s.

Wave dissipation related to breaking, considering the distribution of foam on the time-exposure image, exhibited a relatively complex pattern (Figure 1). Wave dissipation on the outer bar was relatively weak, certainly because the high-energy wave conditions experienced during the storm on 11 March induced an offshore migration of about 100 m (Almar et al., 2010). Due to the presence of a shoreward propagating accretionary wave, which shed from one of the outer-bar horns during the storm (Almar et al., 2010), an isolated patch of light foam between the inner bar and the outer bar can however be observed. Overall, waves were essentially breaking on the inner bar, as denoted by the intense foam observed on Figure 1. However, the presence of a relatively deep channel between the upper beach and the inner bar weakened and even interrupted the breaking process at some cross-shore locations, thus leading to a second breaking point on the lower beach face.

To evaluate the distance over which waves were dissipating through the wave breaking process, the effective surf zone width has been estimated as the distance between the onshore limit of the inner bar where the wave dissipation weakened or stopped and the lower limit on the beach face where wave breaking strengthened or started again. This distance was then subtracted from the distance between the shoreline and the outer breaking point, used as proxy of the inner bar. Figure 3 (middle panel) illustrates the alongshore variability of the morphology: the alongshore range of shoreline-bar distance (black line) was up to 85 m accounting for an increase of 170% from the smallest (observed at alongshore position 25 m corresponding to transect T7) to the highest value (observed at alongshore position −175 m corresponding to transect T4). The effective surf zone width (gray line) ranged from 60 (transect T7) to nearly 200 m (transect T4),

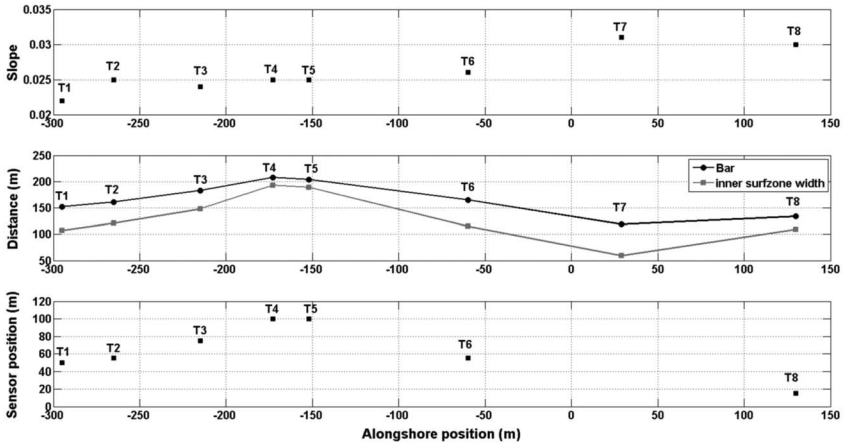

Figure 3. Morphological parameters. (upper) Foreshore beach slope estimate as the linear slope within the region between ± two standard deviations from the mean runup elevation. (middle) Bar position from the shoreline (black line) and effective surf zone width (grey line). (lower) onshore PUV sensor distances from the bar crest. Transect locations are indicated close to the marks.

accounting for an increase of 330% from the smallest to the highest value. The lower beach face also exhibited a complex 3D pattern with the presence of a sandwave between transects T1 and T6 (Figure 1).

3.2. Alongshore Variability in Runup and Surf Zone Statistics

Figure 4 illustrates the topography of the swash zone with the positions of different transects where runup was estimated and the beach profile at each transect. No beach cusps were observed during the field experiment, and the upper beach face was relatively uniform in the alongshore direction. The lower beach face presented a more complex morphology with the presence of the previously mentioned sandwave. Beach profiles exhibited concave profiles, and $\beta_{2\sigma}$ slopes were relatively gentle, typically less than 0.032 (Figure 3, upper panel), consistent with the highly dissipative conditions experienced previously and during the selected period coinciding with low tide. The alongshore range of foreshore beach slope was less than

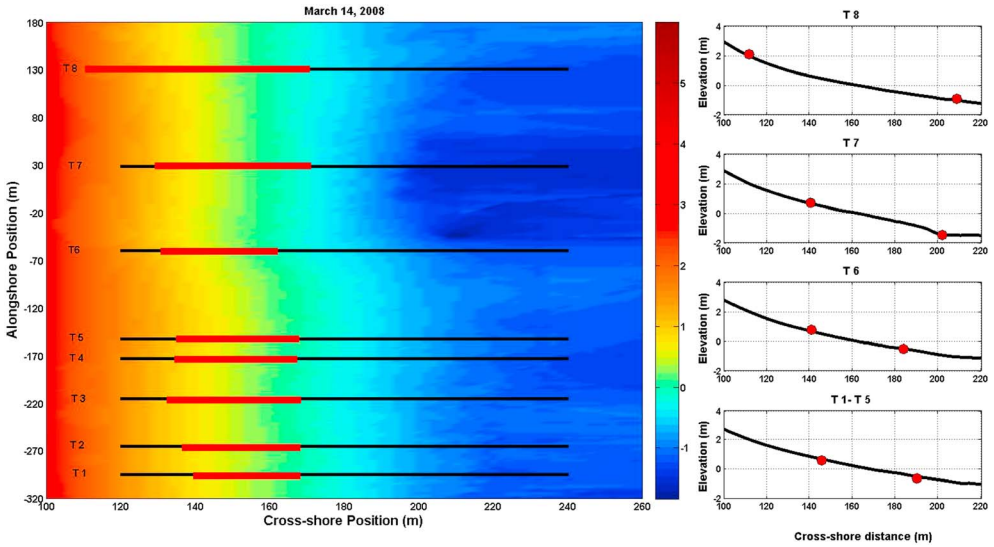

Figure 4. (left) Topographic survey of the low tide swash zone on 14 March and (right) associated beach profiles. The red lines represent the maximum horizontal excursion observed at each transect. The red circles indicate the maximum position reached by the uprush and the downrush along each transect. Note that only one profile is provided for T1–T5 as no significant difference was observed between the different profiles.

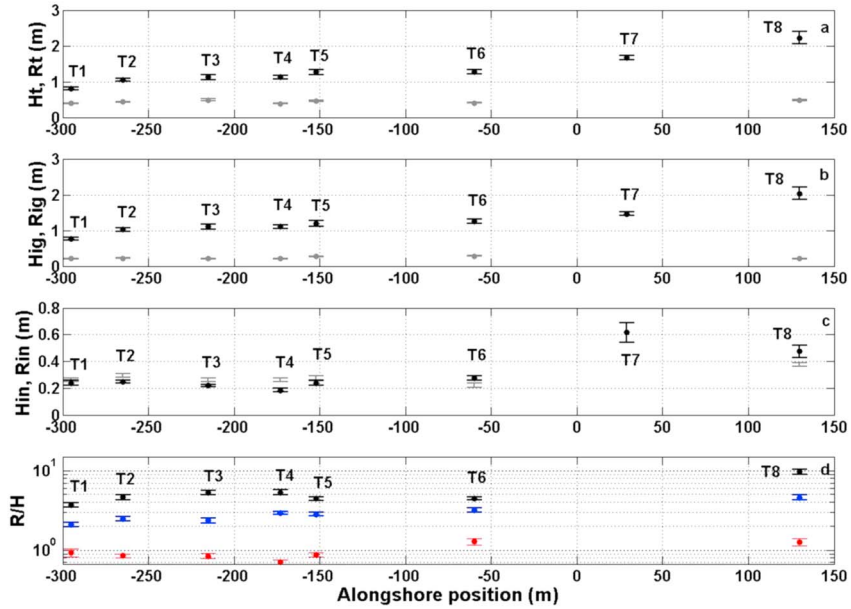

Figure 5. Alongshore variability of wave and runup parameters. (a) Total, (b) infragravity, and (c) incident components of runup elevations (black symbols) and at *surf zone* PUV locations (gray location). (d, log-scale) Ratio R/H for different frequency bands: (blue) total, (black) infragravity, and (red) incident. Vertical bars represent the standard deviation associated with each value. Transect locations are indicated near the marks.

0.010 accounting for an increase of 43% from the smallest to the highest value. Onshore and offshore limits (mean ± 2 standard deviations) of runup excursion for each transect are indicated by circles on the topographic profiles and by the red solid line on the topography (Figure 4). The horizontal excursion of runup is relatively short for transects T1–T6 (typically less than 40 m) but can extend up to 100 m at transect T8. Figure 5 shows the alongshore series of runup parameters as well as surf zone parameters estimated at the PUV sensor locations (see also supporting information for each individual estimate). Data indicate that runup energy is clearly dominated by infragravity energy. Calculated ratios of R_{ig}/R_{in} (not shown) are all above 3. In contrast, surf zone energy is relatively uniformly distributed between the incident and the infragravity band with calculated ratios of H_{ig}/H_{in} (not shown) close to 1. A consistent alongshore and statistically significant (using Snedecor and Student test) trend is observed between transect T1 (alongshore position −300 m) and transect T8 (alongshore position 130 m) for total runup elevation R_t (black symbols) with values normally lower at transects T1–T4 situated on the sandwave (Figure 1) and then increasing toward transect T8 (situated onshore of the rip channel). The increase in total runup elevation is driven both by the increase in the infragravity components and a clear increase in the incident component at transects T7 and T8. Alongshore ranges in R_t and R_{ig} were respectively up to 1.5 and 1.4 m (accounting for an increase of about 300%). Conversely, surf zone parameters (gray symbols) show a remarkably uniform trend with alongshore ranges in H_t and H_{ig} being less than 0.1 m accounting for an increase of less than 130% (statistically significant). Alongshore ranges in R_{in} and H_{in} were respectively up to 0.4 m and less than 0.1, respectively (accounting for an increase of 300% and 150%, respectively). However, variations in H_{in} should be considered relative to their position in the surf zone. Indeed, even if the PUV sensors were situated at the same cross-shore position, their positions within the surf zone were different (Figure 3, lower panel). While PUV4 and PUV5 were well inside the surf zone, PUV8 was close to the breaking zone.

Estimates of the ratio R/H for different frequency bands (Figure 5d) indicate that alongshore variations in runup parameters are not directly correlated with the small alongshore variations in surf zone parameters. Indeed, we observe significant alongshore variations in the R_{ig}/H_{ig} ratio associated with an alongshore range up to 6.5 accounting for an increase of 300% between the lowest and the highest values, while alongshore variations in the R_t/H_t ratio are associated with an alongshore range up to 2.7 accounting for an increase of 237%.

Table 1
Proportion of the Total Variance in the Space-Time Series χ Explained by Their Temporal P_t and Spatial P_y Contributions

χ	P_t	P_y
R_t	0.04	0.87
R_{ig}	0.06	0.83
R_{in}	0.04	0.82
R_{ig}/R_{in}	0.09	0.65
H	0.29	0.58
H_{ig}	0.14	0.66
H_{in}	0.28	0.72
R_t/H_t	0.09	0.80
R_{ig}/H_{ig}	0.07	0.83
R_{in}/H_{in}	0.14	0.59

Following Guedes et al. (2012), in order to evaluate the possible competing role of the alongshore versus temporal variability in the runup and surf zone parameters, the proportion of the total variance explained by the temporal P_t and spatial P_y components were defined as follows:

$$P_t = \frac{\overline{[\langle \chi(t,\ y)\rangle - \chi_m]^2}}{\left\langle [\chi(t,y) - \chi_m]^2 \right\rangle} \tag{3}$$

$$P_y = \frac{\left\langle \left[\overline{\chi(t,y)} \ - \chi_m\right]^2 \right\rangle}{\left\langle [\chi(t,\ y) - \chi_m]^2 \right\rangle} \tag{4}$$

where χ is a generic runup or surf zone parameter, overbar and angle bracket denote, respectively, temporal and spatial averages, and subscript m denotes the average over the whole data set. The results are reported in Table 1. The spatial contributions to the total variance P_y were always greater than the temporal contributions P_t for all runup and surf zone parameters. Concerning the runup parameters, the spatial contribution P_y was an order of magnitude higher than the temporal contribution P_t except for the ratio of infragravity over incident runup elevation R_{ig}/R_{in} that was a factor of 5 higher. Concerning the surf zone parameters, the spatial contribution P_y was a factor of 2 to 5 higher than the temporal contribution P_t; however, given that the sensors were at different depths and not situated at the same location within the surf zone, alongshore variability can be biased. Concerning the ratio between runup and surf zone parameters R/H, the spatial contribution was an order of magnitude higher than the temporal contribution except for the incident frequency band that was a factor of 6.

The influence of surf zone parameters on the swash parameters was further investigated using regression analysis to relate alongshore variability in swash zone parameters to alongshore variability in surf zone parameters (Table 2). Significant correlations were found between runup elevations in the different frequency components and incident surf zone elevations with correlation coefficients around 0.48 (all significant with p value < 0.01) consistent with previous observations (Senechal et al., 2013). Our data also indicate that there is no linear correlation between runup elevation in the infragravity component and infragravity energy in the surf zone when considering all the transects. However, considering linear regression along each transect allows two sections to be distinguished: one section from T1 to T4 where no significant or weak (even if significant) correlation is observed between runup and surf zone parameters and a second section from T5 to T8 (apart from T7) where significant correlation is observed between runup and surf zone parameters.

3.3. Runup and Surf Zone Spectra

Figure 6 shows the averaged runup spectra and the averaged surf zone elevation spectra calculated over the 4-hr window at the different alongshore positions. Averaged spectra were calculated averaging all the 15-min time series for each transect, resulting in 30 degrees of freedom with a bandwidth of 0.0011 Hz. Not only did the relative magnitude between the incident and infragravity runup bands change alongshore but also the shape of the spectra. For all transects, the average runup spectra reveal a saturated region that decayed approximately as f^{-3} (apart from T7 that decayed at approximately $f^{-5/2}$), consistent with previous observations (Guza & Thornton, 1982; Ruessink et al., 1998). The knickpoint between the saturated and unsaturated part was estimated using the method described by Ruessink et al. (1998). The knickpoint found for the present data set ranged from approximately 0.021 to 0.033 Hz with a mean of 0.025 Hz for the runup spectra; that is, the saturated tail of the spectra extended into the infragravity-frequency band ($f < 0.05$ Hz) consistent with previous observations (Ruessink et al., 1998; Ruggiero et al., 2004). One of the most obvious features in the runup spectra are the overall increase of magnitude in infragravity energy from T1 to T8. We observe the presence of energy peaks at very low frequencies, approximately 0.0056 (180 s) and 0.015 Hz (60 s) in the region of the *sandwave* (transects T1–T5) while other transects are characterized by a relatively white spectrum at

Table 2
Linear Regression Results Relating Dependent Runup Variables to Surf Zone Variables Including Slope (m), Offset (b), and Correlation Coefficient (r^2)

	Dependent variable	Independent variables	m	b	r^2
All transects	R_t	H_t	4.15	−0.63	**0.21**
		H_{ig}	1.15	0.11	0.00
		H_{in}	5.87	−0.46	**0.45**
	R_{ig}	H_t	3.87	−0.61	**0.19**
		H_{ig}	0.95	0.50	0.00
		H_{in}	5.39	−0.43	**0.41**
	R_{in}	H_t	0.86	−0.13	**0.17**
		H_{ig}	−0.19	0.29	0.00
		H_{in}	1.39	−0.14	**0.48**
	R_t	H_t	0.90	0.55	**0.12**
		H_{ig}	1.07	0.70	0.03
		H_{in}	0.34	0.84	0.01
T1–T4	R_{ig}	H_t	0.89	046	**0.08**
		H_{ig}	0.81	0.66	0.01
		H_{in}	0.55	0.69	0.01
	R_{in}	H_t	0.16	0.13	0.04
		H_{ig}	0.27	0.14	0.02
		H_{in}	0.45	0.08	**0.09**
	R_t	H_t	7.31	−1.78	**0.34**
		H_{ig}	−10.11	4.06	**0.44**
		H_{in}	6.09	−028	**0.62**
T5–T8	R_{ig}	H_t	6.51	−1.53	**0.32**
		H_{ig}	−8.96	3.66	**0.41**
		H_{in}	5.45	−0.20	**0.59**
	R_{in}	H_t	1.61	−0.42	**0.29**
		H_{ig}	−2.48	0.94	**0.46**
		H_{in}	1.41	−0.10	**0.59**

Note. Regression correlations that are significant at the 99% confidence level are showed in bold. Transect T7 is not included as no PUV sensor was deployed along this transect.

infragravity frequencies (transects T6–T8). Surf zone averaged spectra also reveal a saturated tail but at high frequencies (typically frequencies greater than $5f_p$ where f_p is the incident peak frequency). We also observe the presence of energy peaks in the infragravity band, approximately at 0.015 Hz (60 s) for all transects and around 0.0056 Hz at transects T3 to T6.

4. Discussion

We have presented new observations of wave runup during energetic and stationary offshore wave conditions and in the presence of a complex 3D morphology featuring significant alongshore variability. The present data set fills the gap between previous works focusing on large- (e.g., Guedes et al., 2012; Ruggiero et al., 2004) and small-scale (e.g., Bryan & Coco, 2010) alongshore variable morphologies. One of the novelties arising from the present data set is that alongshore variations in runup under stationary offshore conditions are much higher than what has been reported previously in the literature. Also, the importance of other environmental parameters (e.g., foreshore beach slope) appears to be much lower than what has previously been reported. Alongshore variation in $\beta_{2\sigma}$ was substantially lower than the ones previously reported in studies focusing on alongshore variability in swash motions (e.g., Guedes et al., 2012; Ruggiero et al., 2004). Furthermore, the observed mean alongshore value of $\beta_{2\sigma}$ slopes in this study fills the gap between the extremely dissipative conditions experienced in Ruggiero et al. (2004) and the more reflective conditions experienced in Guedes et al. (2012). Alongshore variations in $\beta_{2\sigma}$ were essentially due to the presence on one hand of the deep channel close to T7 and on the other hand due to the sandwave at T1–T6 (Figures 1). Under dissipative conditions, Ruggiero et al. (2004) reported that runup height could vary by a factor of 2 in the presence of beach slope that varied by a factor of 5. In contrast, during more reflective conditions, Guedes et al. (2012) reported variations in runup by a factor of 1.8 in the presence of beach slope that varied by a factor of 2. In the present data set, variations in runup height are close to a factor of 3 while variations in beach slope are around a factor of 1.6. Our data clearly show that there is a strong variability in the runup observations. However, Figure 7 illustrates that the range of the variability is consistent with previous published observations on the same field area (Senechal, Coco, et al., 2011; Senechal et al., 2013). Senechal, Coco, et al. (2011, black symbols) extracted runup time series along two transects at high tide around and during the major storm that occurred a few days before the period covered in the present study (Figure 2). Their data set covered mild ($H_s \sim 1$ m) to very energetic long swells ($H_s > 6$ m and $T_p \sim 16.4$ s) impinging on steep foreshore beach slopes (0.05–0.08). Senechal et al. (2013, gray symbols) focused on the tidal effects on runup by analyzing runup time series extracted both at high and low tide under stationary offshore conditions along four transects (T3–T6) and partially covered the temporal window discussed in the present study. In particular, they found that the drop in the infragravity component between high and low tide was associated with a drop of the infragravity energy in the inner surf zone, highlighting the possible role of the water level over the bar. Nevertheless, while the range of variability was previously related to a wide range of wave conditions (Senechal, Coco, et al., 2011) or to the tidally controlled water level (Senechal et al., 2013), here the range of variability cannot be ascribed either to the offshore wave characteristics or to the change in the water level.

Interestingly, our data set also shows that alongshore variations in runup are not principally controlled by changes in the slope of the beach face $\beta_{2\sigma}$ (Figure 8) in contrast with previous studies focusing on alongshore variation under stationary offshore conditions (e.g., Guedes et al., 2012; Ruggiero et al., 2004). Guedes et al. (2012) showed that under mild, swell-dominated offshore wave conditions, alongshore variations in runup were mainly controlled by the slope of the beach face $\beta_{2\sigma}$. However, in their data set, the significant runup height R was predominantly driven by energy at the incident frequencies in contrast to our data set where

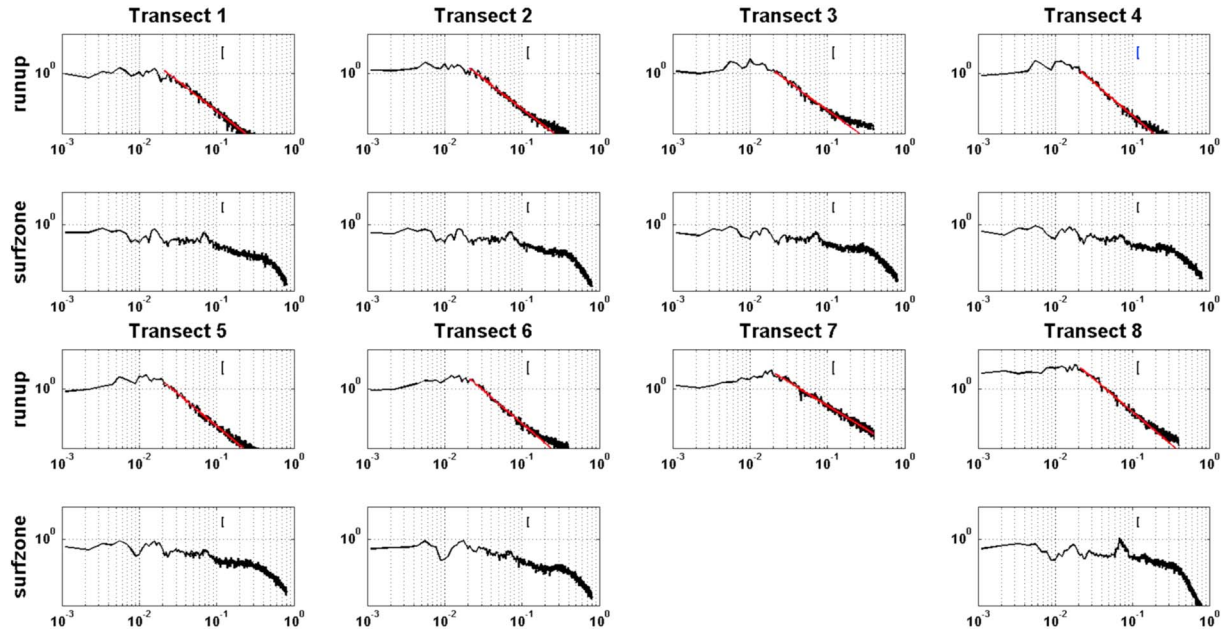

Figure 6. Runup and surf zone energy averaged density spectra at the different transects. The vertical bar is the 99% confident interval. The red lines represent the best fits to the estimate in the log-log space of the saturated part.

runup height was dominated by energy at infragravity frequencies. Under highly dissipative conditions, Ruggiero et al. (2004) found the runup height R to be dominated by energy at infragravity frequencies and linearly dependent on the local foreshore beach slope $\beta_{2\sigma}$ that varied by a factor of 5. However, that is much more than in the present data set where the local foreshore beach slope $\beta_{2\sigma}$ varied by a factor of less than 2. As previously pointed out by Senechal, Coco, et al. (2011), the choice of the foreshore beach slope defined as $\beta_{2\sigma}$ might not be suitable as it does not represent the whole cross-shore profile, particularly in the surf zone. Indeed, recent works (e.g., Gomes da Silva et al., 2018; Hughes et al., 2014) indicated that both the profile shape and the morphodynamic beach state should be considered. However, both authors used qualitative parameters (not directly taking into account the beach slope) to represent the 3D large-scale morphology pattern of the beach: while Hughes et al. (2014) used the beach classification proposed by Wright et al. (1984), Gomes da Silva et al. (2018) proposed to use the nondimensional fall velocity parameter. In this study, an additional difficulty is related to the presence of the sandwave creating a much milder and homogenous surf zone slope in the area that also likely influences the runup.

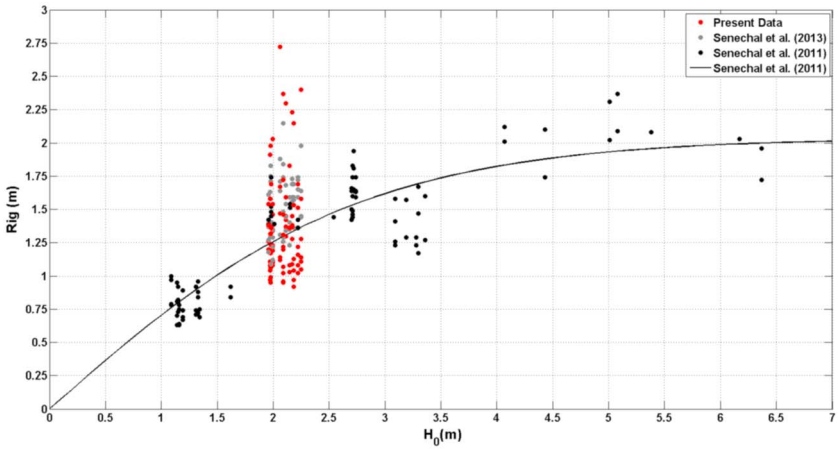

Figure 7. Present data set (red marks) compared to previous data acquired in the same area with the same methodology (gray and black marks).

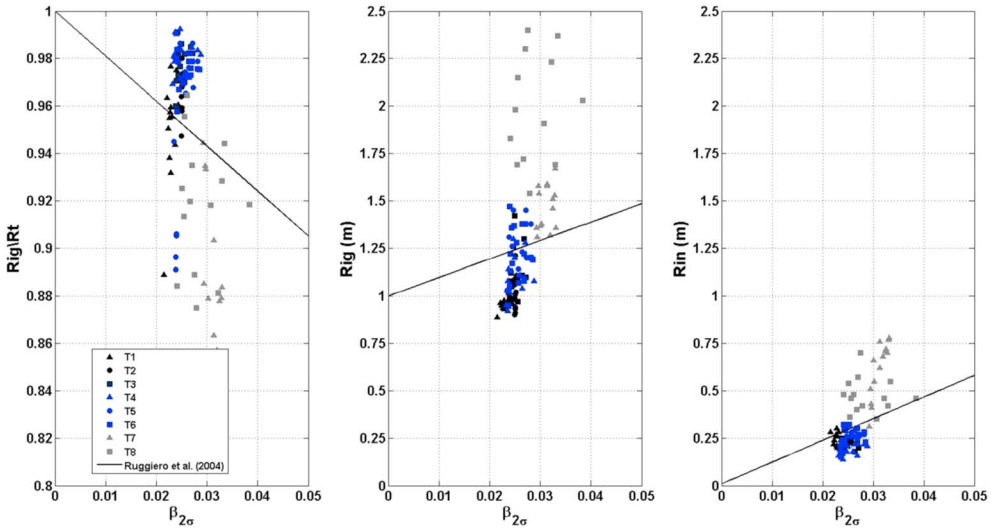

Figure 8. Infragravity runup (left and middle panels) and incident runup (right) versus foreshore beach slope for all the transects. The black lines represent the best-fit lines proposed by Ruggiero et al. (2004).

Specifically, Figure 8 highlights that most of the alongshore variability is driven by the data at T7 and T8 (gray marks) not situated in the area of the sandwave in contrast to the other transects. Alongshore variability is observed at both the infragravity (middle) and incident (right) bands of frequencies. In particular (see also Figure 5), energy at incident frequencies is significantly higher at T7 and T8. This could be related to the energy dissipation patterns observed in the surf zone. Indeed, transect T7 is associated with both the shortest effective surf zone and the steepest foreshore slope due to the presence of the deepest part of the rip channel (Figure 3); this might enhance the incident component of the runup energy. Figure 9 represents alongshore timestacks generated from the video images at different cross-shore locations all situated between the inner bar and the shoreline. We observe that the energy dissipation pattern presents a significant alongshore variability. In particular, at transect T7 we clearly observe that waves are not breaking continuously from the inner bar to the shore while at transect T2 waves are breaking nearly continuously. This is consistent with previous work reporting that in the presence of a barred beach, the runup magnitude at incident frequencies can range by up to an order of magnitude between low and high tides (Guedes et al., 2011) or as a result of alongshore variability (Guedes et al., 2012). These variations were driven by variation in the degree of wave dissipation attributed either to tidal modulation in wave energy dissipation (Guedes et al., 2011) or to the bar morphology (Guedes et al., 2012) that ultimately controlled the energy driving the runup and hence its amplitude.

However, visual observations of the instantaneous images also suggest that a strong wave refraction pattern is observed around the sandwave observed on the lower beach face (Timex in Figure 1 and Snapshot in Figure 9), leading to wave energy focusing on its southern side where transect T7 is situated. This has been further investigated using the wavenumber estimation methods based on fitting the cross-spectral correlation (Plant et al., 2008). The results are shown in Figure 10. The results are plotted for the 0.067-Hz frequency that corresponds to the peak energy measured at the PUV sensor in the incident band of frequencies (Figure 6) and corresponded to video-imaged variability that was coherent enough to extract wave-propagation patterns. The wavenumber (Figure 10a) is robustly estimated in much of the domain around the sandwave pattern, indicated by error predictions (Figure 10c, showing the root mean square error of the wavenumber estimate) that are generally much smaller than the estimated wavenumbers. The directions of wave approach (Figure 10b) are estimated robustly in the inner portion of the analysis region, with root mean square angle errors typically less than the magnitude of the angles (Figure 10d). They show a remarkable alongshore gradient, with waves on the northern side of the sandwave pattern (located between alongshore positions −250 and −50 m) approaching the shoreline with a negative angle, consistent with the offshore North-West incidence of the waves while waves on the

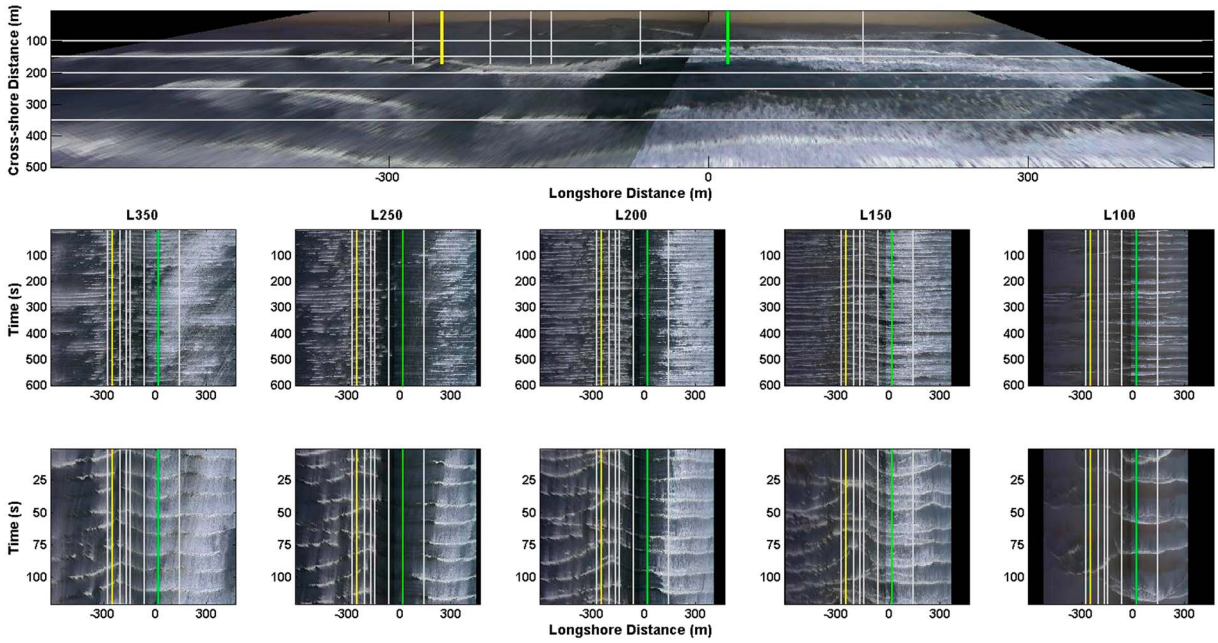

Figure 9. (upper panel) Snapshot with positions of the different cross-shore transects (grey vertical lines) and the longshore transects (grey horizontal lines). The yellow and green lines represent the T2 and the T7 transects, respectively. (middle panels) 600 s alongshore timestacks generated at different alongshore positions (100, 150, 200, 250, and 350 m) and (lower panels) 120-s enlargement view.

southern side of the sandwave pattern are approaching the shoreline with a positive angle (South-West incidence).

While field evidence indicate that alongshore variations in the incident runup can be explained by variation in the degree of energy dissipation and possibly by wave refraction patterns, runup still remains dominated by the energy at infragravity frequencies. In the absence of well-developed beach cusps that can affect swash characteristics (e.g., Bryan & Coco, 2010; Ciriano et al., 2005), alongshore variations in infragravity runup have largely been attributed to beach face slope variations, a hypothesis that for our data does not hold. However, Guedes et al. (2011) provided evidence of the presence of secondary waves (harmonic released waves) that might be related to an increase in the energy at infragravity frequencies. We clearly observe in our data that there is an increasing number of wave crests in the area where transects T7 and T8 are located, resulting in more crests progressing across the beach face in contrast to the area where transects T1 to T5 are located (Figure 9, L150 and L100). We also observe that these secondary waves might then be merging with the primary ones when propagating in the swash zone. Merging bores have been previously reported to be one possible mechanism of infragravity wave generation mechanism in the inner surf zone (e.g., Senechal et al., 2001). However, very recently, Tissier et al. (2017) using both laboratory experiments and numerical modeling showed that bore merging occurs in a part of the surf zone that is already dominated by infragravity energy suggesting that bore merging as an infragravity wave generation mechanism might not be significant. In the present study, even if merging bores are more often observed at locations where infragravity levels are the highest, we are not able to conclude if bore merging is the cause of the effect of infragravity wave generation.

Interestingly, we also observe that the largest horizontal runup excursions measured in our data set were found to occur in front of T7 and T8 (Figure 4). Associated with the highest slopes (Figure 3), they resulted in the largest runup events measured in our data set. Using a numerical model base on the Reynold-averaged Navier-Stokes equations, Garcia-Medina et al. (2017) showed that the largest runup events are associated with bore merging (bore-bore capture) on gently sloping beaches even if they also showed that bore-bore capture is found to be a necessary but not sufficient condition for large runup generation. In particular, they also showed that the phase difference between incident and infragravity waves is also a key factor, explaining up to 30% of the variability in the largest runup.

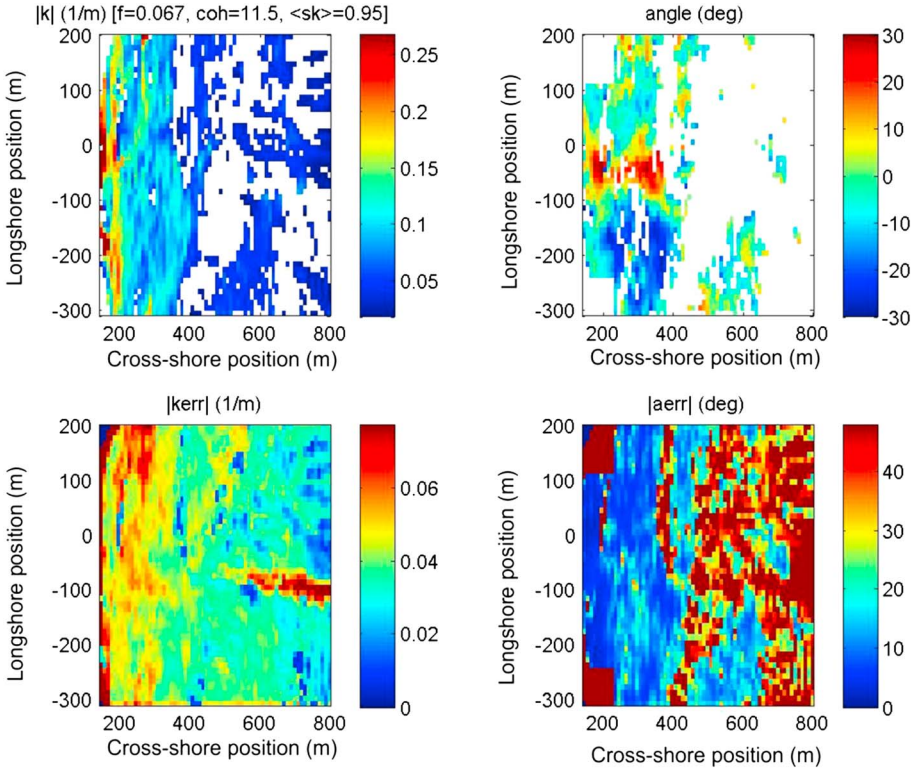

Figure 10. Estimates of wavenumber magnitude (upper left), wave direction (upper right), and predicted errors (lower panels) at frequency 0.067 Hz (14.9 s, peak period in the energy band at incident frequencies). In the upper left and right panels, results are omitted where individual wavenumber/angle estimates explain less than 50% of the cross-spectral variance. The sandwave is located between alongshore positions −250 and −50 m.

Furthermore, the generation of secondary waves (visible in Figure 9 at L250 and L200) and the presence of the deepest section of the channel in front of T7 and T8 might have delayed the energy dissipation on the beach face as observed in Senechal et al. (2002). This is consistent with the ratio R_{in}/H_{in} being higher than 1 at T8 (Figure 5) and the observed shapes of the spectra (Figure 6). Following the synthesis by Hughes et al. (2014), swash spectra at transects T1–T5 are consistent with the swash spectra encountered in the presence of the lower-energy intermediate beach state. They are generally characterized by a peaky structure in the infragravity band with the difference that in the present data the infragravity swash energy is larger than the total short-wave swash energy. In contrast, swash spectra at transects T6–T8 are consistent with the swash spectra encountered in the presence of the higher-energy intermediate and dissipative beach states characterized by a featureless infragravity swash band.

To further investigate the possible role of the sandwave on the alongshore variability in runup, the alongshore length scale of coherence has been estimated both in the surf zone and in the swash zone. In particular, the alongshore length scale of coherence has been used to relate morphological patterns to runup patterns. Following Holland (1995) and Ruggiero et al. (2004), the alongshore structure of infragravity energy has been defined as the length scale over which runup (or pressure) motions of a given frequency are coherent. Squared coherence values were calculated similarly to Ruggiero et al. (2004) from the cross-spectral matrix of all possible runup transect (or pressure sensor) pairs as a function of frequency and transect (sensor) separation (alongshore lag). Figure 11 illustrates the squared coherence calculated at both the runup transects (above) and the PUV sensors (below) for the frequency peaks 0.0154 (left) and 0.0055 Hz (right). We observe that for these two peak frequencies (one is the PUV peak frequency, the other is the peak frequency in the majority of swash spectra), the coherence length scale is approximately 200 m at the shoreline and slightly longer at the PUV sensor (300 m). The value obtained for the peak frequency 0.0055 Hz is much lower than the one found by Ruggiero et al. (2004), which was close to 1,200 m but higher than the one reported by Holland and Holman (1999). The value obtained for the peak frequency

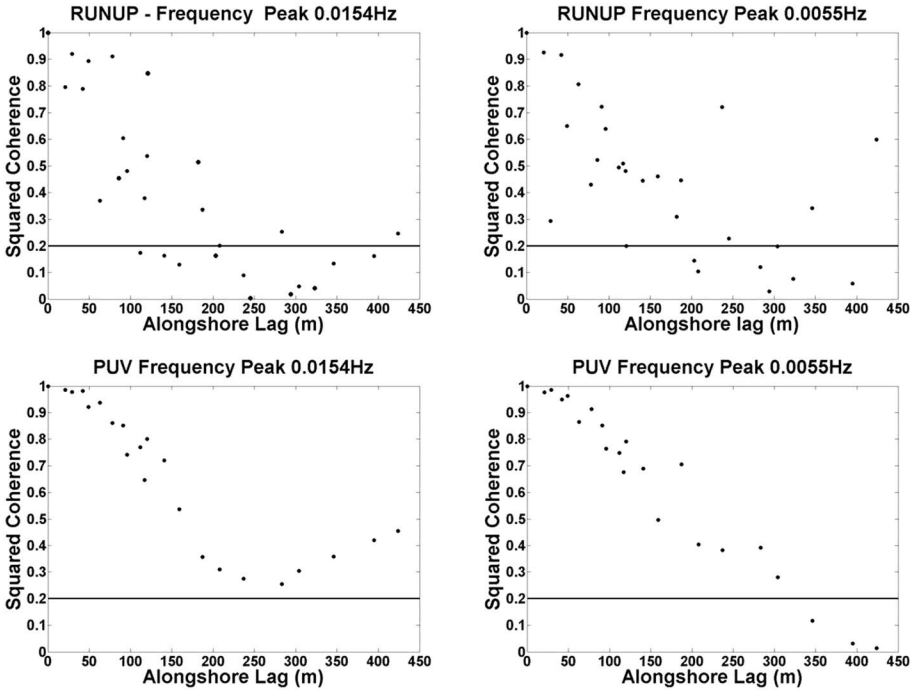

Figure 11. Squared coherence of elevation at the shoreline (above) and at the PUV sensors (below) for two infragravity frequencies. The 95% significance level (solid line) versus alongshore lag for two peak frequencies.

0.0154 Hz is consistent with Ruggiero et al. (2004). The difference cannot be explained by the difference of the sensor array alongshore length: 450 m in the present study versus 1,600 m in Ruggiero et al. (2004) and 260 m in Holland and Holman (1999). Indeed, many peak frequencies show the same pattern with similar values. Ruggiero et al. (2004) indicated that the long alongshore length scales observed in their data set were certainly associated with the environmental conditions during their study characterized by very large morphodynamic and hydrodynamic cross-shore length scales with sandbars typically located up to several hundred meters from the shoreline. In the present study, the cross-shore lengths are very short, and the topography/bathymetry exhibits a complex alongshore pattern whose typical alongshore length is about 250 m (Figure 1, time exposure image), relatively consistent with the typical coherence length scales.

5. Conclusions

Observations of wave runup data derived from video recordings were collected at low tide in the presence of complex beach morphology during stationary energetic conditions characterized by offshore wave heights of 2 m and peak periods of nearly 14 s. Over the study period, variations in runup were found to be largely dominated by the spatial, rather than temporal, dimension allowing us to exclude variations in the offshore wave forcing (significant wave height and period) and closely investigate the effects of other variables. Runup spectra estimated at different alongshore positions were always dominated by infragravity energy and showed a broad saturated region with an f^{-3} dependence extending in the infragravity band.

Runup height varied by a factor 3, a much higher value than the one reported previously in the literature (e.g., Guedes et al., 2012; Ruggiero et al., 2004), while variations in environmental parameters (e.g., foreshore beach slope) were much lower. While previous alongshore variability in runup heights was essentially ascribed to the foreshore beach slope (e.g., Guedes et al., 2012; Ruggiero et al., 2004), here the beach morphology in the inner surf zone seems to play a crucial role. In particular, the 3D patterns exhibited by the morphology led to rapid modification in the incident wave patterns over a short cross-shore distance. For example, wave refraction around the sand pattern led to increased incident energy level in the runup spectra at specific alongshore locations. The alongshore coherence length scales were consistent with the typical alongshore

length scale of the morphology. Further work is needed as we still struggle to understand and predict how the morphology affects runup, a key driver of coastal inundation.

Acknowledgments

We wish to thank all the organizations that have provided financial support for the field experiment, in particular the French DGA (ECORS project). Thanks also to Rafael Almar, George Payne, Vincent Marieu, and Antoine Réjas for the support in the installation of the video system; and to Jean-Paul Parisot, Sylvain Capo, and Stephan Bujan for the Real Time Kinematic Differential Global Positioning System data. The raw data used (video images and pressure sensors) can be obtained by directly contacting the corresponding author. The data generated (video extracted runup, etc.) are provided in the supporting information. Finally, the authors are grateful for the detailed suggestions and constructive comments provided by Peter Ruggiero, the other anonymous reviewer, and the Associate Editor that vastly improved this manuscript.

References

Almar, R., Castelle, B., Ruessink, B. G., Senechal, N., Bonneton, P., & Marieu, V. (2010). Two- and three-dimensional double-sandbar system behaviour under intense wave forcing and a meso-macro tidal range. *Continental Shelf Research*, *30*(7), 781–792. https://doi.org/10.1016/j.csr.2010.02.001

Arns, A., Dangendorf, S., Jense, J., Talke, S., Bender, J., & Pattiaratchi, C. (2017). Sea-level rise induced amplification of coastal protection design heights. *Scientific Reports*, *7*(1), 40171. https://doi.org/10.1038/srep40171

Atkinson, A. L., Power, H. E., Moura, T., Hamond, T., Callagha, D. P., & Baldock, T. E. (2017). Assessment of runup predictions by empirical models on no-truncated beaches on the south-east Australian coast. *Coastal Engineering*, *119*, 15–31. https://doi.org/10.1016/j.coastaleng.2016.10.001

Battjes, J. A. (1974). Surf similarity. In *Proceedings of 14th Coastal Engineering Conference* (pp. 466–480). Copenhagen – Denmark.

Blenkinsopp, C. E., Matias, A., Howe, D., Castelle, B., Marieu, V., & Turner, I. L. (2016). Wave runup and overwash on a prototype-scale sand barrier. *Coastal Engineering*, *113*, 88–103. https://doi.org/10.1016/j.coastaleng.2015.08.006

Briganti, R., Bellotti, G., Franco, L., De Rouck, J., & Geeraerts, J. (2005). Field measurements of wave overtopping at the rubble mound breakwater of Rome-Ostia yacht harbor. *Coastal Engineering*, *52*(12), 1155–1174. https://doi.org/10.1016/j.coastaleng.2005.07.001

Bryan, K. R., & Coco, G. (2010). Observations of nonlinear runup patterns on plane and rhythmic beach morphology. *Journal of Geophysical Research*, *115*, C09017. https://doi.org/10.1029/2009JC005721

Butel, R., Dupuis, H., & Bonneton, P. (2002). Spatial variability of wave conditions on the French Aquitanian coast using in-situ data. *Journal of Coastal Research*, *SI36*, 96–108.

Castelle, B., Bonneton, P., Dupuis, H., & Sénéchal, N. (2007). Double bar beach dynamics on the high energy meso-macrotidal French Aquitanian coast: A review. *Marine Geology*, *245*(1-4), 141–159. https://doi.org/10.1016/j.margeo.2007.06.001

Ciriano, Y., Coco, G., Bryan, K. R., & Elgar, S. (2005). Field observations of swash zone infragravity motions and beach cusp evolution. *Journal of Geophysical Research*, *110*, C02018. https://doi.org/10.1029/2004JC002485

Coco, G., Werner, B. T., Burnet, T., & Elgar, S. (2004). The role of tides in beach cusp formation. *Journal of Geophysiscal Research*, *109*, CO4011. https://doi.org/10.1029/2003JC002154

Cohn, N., & Ruggiero, P. (2016). The influence of seasonal to interannual nearshore profile variability on extreme water levels: Modelling wave runup on dissipative beaches. *Coastal Engineering*, *115*, 79–92. https://doi.org/10.1016/j.coastaleng.2016.01.006

Cox, N., Dukin, L. M., & Irish, J. L. (2013). An empirical model for infragravity swash on barred beaches. *Coastal Engineering*, *81*, 44–50. https://doi.org/10.1016/j.coastaleng.2013.06.008

De Bakker, A. T. M., Tissier, M. F. S., & Ruessink, B. G. (2014). Shoreline dissipation of infragravity waves. *Continental Shelf Research*, *72*, 73–82. https://doi.org/10.1016/j.csr.2013.11.013

De Bakker, A. T. M., Tissier, M. F. S., & Ruessink, B. G. (2015). Beach steepness effects on nonlinear infragravity-wave interactions: A numerical study. *Journal of Geophysical Research: Oceans*, *121*, 554–570. https://doi.org/10.1002/2015JCO11268

Elfrink, B., & Baldock, T. (2002). Hydrodynamics and sediment transport in the swash zone: A review and perspectives. *Coastal Engineering*, *45*(3-4), 149–167. https://doi.org/10.1016/S0378-3839(02)00032-7

Gallagher, E., MacMahan, J. H. M., Reniers, A., Brown, J., & Thornton, E. (2011). Grain size variability on a rip-channeled beach. *Marine Geology*, *287*(1–4), 11.

Garcia-Medina, G., Özkan-Haller, H. T., Holman, R. A., & Ruggiero, P. (2017). Large runup controls on a gently sloping dissipative beach. *Journal of Geophysical Research: Oceans*, *122*, 5998–6010. https://doi.org/10.1002/2017JC012862

Gomes da Silva, P., Medina, R., Gonzalez, M., & Garnier, R. (2018). Infragravity swash parameterization on beaches: The role of the profile shape and the morphodynamic beach state. *Coastal Engineering*, *136*, 41–55. https://doi.org/10.1016/j.coastaleng.2018.02.002

Guedes, R. M. C., Brya, K. R., & Coco, G. (2012). Observations of alongshore variability of swash motions on an intermediate beach. *Continental Shelf Research*, *48*, 61–74. https://doi.org/10.1016/j.csr.2012.08.022

Guedes, R. M. C., Bryan, K. R., Coco, G., & Holman, R. A. (2011). The effects of tides on swash statistics on an intermediate beach. *Journal of Geophysical Research*, *116*, C04008. https://doi.org/10.1029/2010JC006660

Guza, R. T., & Thornton, E. B. (1982). Swash oscillations on a natural beach. *Journal of Geophysical Research*, *87*(C1), 483–491. https://doi.org/10.1029/JC087iC01p00483

Guza, R. T., Thornton, E. B., Holman, R. A. (1984). Swash on steep and shallow beaches, *Paper presented at the 19th Coastal Engineering Conference*, Am. Soc. Of Civ. Eng., Houston, Tex.

Hawkes, P. J., Gouldby, B. P., Tawn, J. A., & Owen, M. W. (2002). The joint probability of waves and water levels in coastal defence design. *Journal of Hydraulic Research*, *40*(3), 241–251. https://doi.org/10.1080/00221680209499940

Herbers, T., & Burton, M. (1997). Nonlinear shoaling of directionally spread waves on a beach. *Journal of Geophysical Research*, *102*(C9), 21,101–21,114. https://doi.org/10.1029/97JC01581

Herbers, T. H. C., Elgar, S., & Guza, R. T. (1995). Generation and propagation of infragravity waves. *Journal of Geophysical Research*, *100*, 24,863–24,872. https://doi.org/10.1029/95JC02680

Holland, K. T. (1995). Foreshore dynamics: swash motions and topographic interactions on natural beaches, Ph.D. thesis, Oreg. State Univ., Corvallis, Oreg.

Holland, K. T., & Holman, R. A. (1999). Wavenumber-frequency structure of infragravity swash motions. *Journal of Geophysical Research*, *104*(C6), 13,479–13,488. https://doi.org/10.1029/1999JC900075

Holland, K. T., Holman, R. A., Lippmann, T. C., Stanley, J., & Plant, N. (1997). Practical use of video imagery in nearshore oceanographic field studies. *Oceanic Engineering, IEEE*, *22*(1), 81–92. https://doi.org/10.1109/48.557542

Holman, R. A. (1986). Extreme value statistics for wave run-up on a natural beach. *Coastal Engineering*, *9*(6), 527–544. https://doi.org/10.1016/0378-3839(86)90002-5

Holman, R. A., & Bowen, A. J. (1984). Longshore structure of infragravity wave motions. *Journal of Geophysical Research*, *89*(C4), 6446–6452.

Holman, R. A., & Sallenger, A. H. (1985). Setup and swash on a natural beach. *Journal of Geophysiscal Research*, *90*(C1), 945–953. https://doi.org/10.1029/JC090iC01p00945

Houser, C. (2009). Synchronization of transport and supply in beach-dune interaction. *Progress in Physical Geography*, *33*(6), 733–746. https://doi.org/10.1177/0309133309350120

Hughes, M. G., Aagaard, T., Baldock, T. E., & Power, H. E. (2014). Spectral signatures for swash on reflective, intermediate and dissipative beaches. *Marine Geology*, *355*, 88–97. https://doi.org/10.1016/j.margeo.2014.05.015

Hughes, M. G., Moseley, A. S., & Baldock, T. E. (2010). Probability distributions for wave runup on beaches. *Coastal Engineering*, *57*(6), 575–584. https://doi.org/10.1016/j.coastaleng.2010.01.001

Lippmann, T. C., & Holman, R. A. (1989). Quantification of sandbar morphology: A video technique based on wave dissipation. *Journal of Geophysical Research*, *94*(C1), 995–1011. https://doi.org/10.1029/JC094iC01p00995

Longuet-Higgins, M. S., & Stewart, R. W. (1962). Radiation stress and mass transport in gravity waves, with applications to 'surf beat'. *Journal of Fluid Mechanics*, *13*(04), 481–504. https://doi.org/10.1017/S0022112062000877

Masselink, G., & Short, A. D. (1993). The effect of tide range on beach morphodynamics and morphology: A conceptual beach model. *Journal of Coastal Research*, *9*, 785–800.

Medellin, G., Brinkkemper, J. A., Torres-Freyermuth, A., Appendini, C. M., Mendoza, E. T., & Salles, P. (2016). Run-up parameterization and beach vulnerability assessment on a barrier island: A downscaling approach. *Natural Hazards and Earth System Sciences*, *16*(1), 167–180. https://doi.org/10.5194/nhess-16-167-2016

Meyer, R. E., & Taylor, A. D. (1972). Run-up on beaches. In R. E. Meyer (Ed.), *Wave on beaches and resulting sediment transport* (pp. 357–411). San Diego, CA: Academic.

Miche, R. (1951). Le pouvoir réfléchissant des ouvrages maritimes exposés à l'action de la houle. *Ann Ponts Chaussées*, *121*, 285–319.

Nicolae Lerma, A., Pedreros, R., Robinet, A., & Senechal, N. (2017). Simulating wave setup and runup during storm conditions on a complex barred beach. *Coastal Engineering*, *123*, 29–41. https://doi.org/10.1016/j.coastaleng.2017.01.011

Nicolae Lerma, A., Pedreros, R., & Senechal, N. (2016). Wave set-up and run-up variability on a complex barred beach during highly dissipative storm conditions. *Journal of Coastal Research*, *SI75*, 882–886.

Norheim, C., Herbers, T., & Elar, S. (1998). Nonlinear evolution of surface wave spectra on a beach. *Journal of Physical Oceanography*, *28*(7), 1534–1551. https://doi.org/10.1175/1520-0485(1998)028<1534:NEOSWS>2.0.CO;2

Okhiro, M., & Guza, R. T. (1995). Infragravity energy modulation by tides. *Journal of Geophysical Research*, *100*(C8), 16,143–16,148. https://doi.org/10.1029/95JC01545

Palmsten, M. L., & Splinter, K. D. (2016). Observations and simulations of wave runup during a laboratory dune erosion experiment. *Coastal Engineering*, *115*, 58–66. https://doi.org/10.1016/j.coastaleng.2016.01.007

Parisot, J. P., Capo, S., Castelle, B., Bujan, S., Moreau, J., Gervais, M., et al. (2009). Evolution of a multi-barred sandy beaches in presence of very energetic events. *Journal of Coastal Research*, *SI56*, 1786–1790.

Passarella, M., Goldstein, E. B., De Muro, S., & Coco, G. (2018). The use of genetic programming to develop a predictor of swash excursion on sandy beaches. *Natural Hazards and Earth System Sciences*, *18*(2), 599–611. https://doi.org/10.5194/nhess-18-599-2018

Peregrine, D. H., & Williams, S. M. (2001). Swash overtopping a truncated plane beach. *Journal of Fluid Mechanics*, *440*, 391–399.

Plant, N. G., Holland, K. T., & Haller, M. C. (2008). Ocean wavenumber estimation from wave-resolving time series imagery. *IEEE Transactions on Geoscience and Remote Sensing*, *46*(9), 2644–2658. https://doi.org/10.1109/TGRS.2008.919821

Plant, N. G., & Stockdon, H. F. (2015). How well can wave runup be predicted? Comment on Laudier et al. (2011) and Stockdon et al. (2006). *Coastal Engineering*, *102*, 44–48. https://doi.org/10.1016/j.coastaleng.2015.05.001

Raubenheimer, B., & Guza, R. T. (1996). Observations and predictions of run-up. *Journal of Geophysiscal Research*, *101*(C11), 25575–25587. https://doi.org/10.1029/96JC02432

Raubenheimer, B., Guza, R. T., Elgar, S., & Kobayashi, N. (1995). Swash on a gently sloping beach. *Journal of Geophysiscal Research*, *100*(C5), 8751–8760. https://doi.org/10.1029/95JC00232

Rodrigues, B. A., Matias, A., & Ferreira, O. (2012). Overwash hazard assessment. *Geologica Acta*, *10*(4), 427–437.

Ruessink, B. G. (1998). The temporal and spatial variability of infragravity energy in a barred nearshore zone. *Continental Shelf Research*, *18*(6), 585–605. https://doi.org/10.1016/S0278-4343(97)00055-1

Ruessink, B. G., Kleinhans, M. G., & Van den Beukel, P. G. L. (1998). Observations of swash under highly dissipative conditions. *Journal of Geophysiscal Research*, *103*(C2), 3111–3118. https://doi.org/10.1029/97JC02791

Ruggiero, P., Holman, R. A., & Beach, R. A. (2004). Wave run-up on a high-energy dissipative beach. *Journal of Geophysical Research*, *109*, C06025. https://doi.org/10.1029/2003JC002160

Ruggiero, P., Komar, P. D., Marra, J. J., McDougal, W. G., & Beach, R. A. (2001). Wave runup, extreme water levels and the erosion of the properties backing beaches. *Journal of Coastal Research*, *17*, 407–419.

Ruju, A., Lara, J. L., & Losada, I. J. (2014). Numerical analysis of runup oscillations under dissipative conditions. *Coastal Engineering*, *86*, 45–56. https://doi.org/10.1016/j.coastaleng.2014.01.010

Sallenger, A. H. (2000). Storm impact scale for barrier islands. *Journal of Coastal Research*, *16*(3), 890–895.

Senechal, N., Abadie, S., Ardhuin, F., Gallagher, E., MacMahan, J. H. M., Masselink, G., et al. (2011). The ECORS-Truc Vert'08 field beach experiment: Presentation of a three-dimensional morphologic system in a macro-tidal environment during consecutive extreme storm conditions. *Ocean Dynamics*, *61*(12), 2073–2098. https://doi.org/10.1007/s10236-011-0472-x

Senechal, N., Bonneton, P., & Dupuis, H. (2002). Field experiment on secondary wave generation on a barred beach and the consequent evolution of energy dissipation on the beach face. *Coastal Engineering*, *46*(3), 233–247. https://doi.org/10.1016/S0378-3839(02)00095-9

Senechal, N., Coco, G., Bryan, K., MacMahan, J., Brown, J., & Holman, R. (2013). Tidal effects on runup in the presence of complex 3D morphologies and dissipative surf zone conditions. In P. Bonneton & T. Garlan (Ed.), *Proceedings of Proceedings of the 7th International Conference on Coastal Dynamics* (pp. 325–326).

Senechal, N., Coco, G., Bryan, K. R., & Holman, R. A. (2011). Wave runup during extreme storm conditions. *Journal of Geophysical Research*, *116*, C07032. https://doi.org/10.1029/2010JC006819

Senechal, N., Dupuis, H., Bonneton, P., Howa, H., & Pedreros, R. (2001). Observation of irregular wave transformation in the surf zone over a gently sloping beach on the French Atlantic coastline. *Oceanologica Acta*, *24*(6), 545–556. https://doi.org/10.1016/S0399-1784(01)01171-9

Senechal, N., Gouriou, T., Castelle, B., Parisot, J. P., Capo, S., Bujan, S., & Howa, H. (2009). Morphodynamic response of a meso- to macro-tidal intermediate beach based on a long-term data-set. *Geomorphology*, *107*(3-4), 263–274. https://doi.org/10.1016/j.geomorph.2008.12.016

Serafin, K. A., & Ruggiero, P. (2014). Simulating extreme total water levels using a time-dependent, extreme value approach. *Journal of Geophysical Research: Oceans*, *119*, 6305–6329. https://doi.org/10.1002/2014JC010093

Stockdon, H. F., Holman, R. A., Howd, P. A., & Sallenger, A. H. Jr. (2006). Empirical parameterization of setup, swash and runup. *Coastal Engineering*, *53*(7), 573–588. https://doi.org/10.1016/j.coastaleng.2005.12.005

Stockdon, H. F., Sallenger, A. H., Holman, R. A., & Howd, P. A. (2007). A simple model for the spatially-variable coastal erosion to hurricanes. *Marine Geology*, *238*(1-4), 1–20. https://doi.org/10.1016/j.margeo.2006.11.004

Stockdon, H. F., Thompson, D. M., Plant, N. G., & Long, J. W. (2014). Evaluation of wave runup predictions from numerical and parametric models. *Coastal Engineering*, *92*, 1–11. https://doi.org/10.1016/j.coastaleng.2014.06.004

Suanez, S., Blaise, E., Cancouët, R., & Floc'h, F. (2016). Empirical parameterization of wave ruup and dune erosion during storm conditions on a natural macrotidal beach. *Journal of Coastal Research*, *SI75*, 932–936.

Suanez, S., Cancouêt, R., Floc'h, F., Blaise, E., Ardhuin, F., Filipot, J. F., et al. (2015). Observations and predictions of wave runup, extreme water levels, and medium-term dune erosion during storm conditions. *Journal of Marine Science and Engineering*, *3*(3), 674–698. https://doi.org/10.3390/jmse3030674

Thomson, J., Elgar, S., Raubenheimer, B., Herbers, T. H. C., & Guza, R. T. (2006). Tidal modulation of infragravity waves via nonlinear losses in the surfzone. *Geophysical Research Letters*, *33*, L05601. https://doi.org/10.1029/2005GL025514

Tissier, M., Bonneton, P., & Ruessink, G. (2017). Infragravity waves and bore merging. In T. Aagaard, R. Deigaard, & D. Fuhrman (Eds.), *Proceedings of coastal dynamics* (pp. 451–460). Retrieved from http://coastaldynamics2017.dk/proceedings.html

Van Enckevort, I. M. J., & Ruessink, B. G. (2001). Effect of hydrodynamics and bathymetry on video estimates of nearshore sandbar position. *Journal of Geophysical Research*, *106*(C8), 16,969–16,979. https://doi.org/10.1029/1999JC000167

Van Gent, M. R. A., & Giarrusso, C. C. 2005. Influence of foreshore mobility on wave boundary conditions. *Proceedings WAVES 2005*.

Vousdoukas, M. I., Wziatek, D., & Almeida, L. P. (2012). Coastal vulnerability assessment based on video wave runup observations at a mesotidal, steep-sloped beach. *Ocean Dynamics*, *62*(1), 123–137. https://doi.org/10.1007/s10236-011-0480-x

Wright, L. D., Short, A. D., & Green, M. O. (1984). Morphodynamic variability of surf zones and beaches: A synthesis. *Marine Geology*, *56*(1-4), 93–118. https://doi.org/10.1016/0025-3227(84)90008-2